Article

Discovery of a selective allosteric inhibitor targeting macrodomain 2 of poly-adenosine-diphosphate-ribose polymerases 14

Marion Schuller, Kerstin Riedel, Ian Gibbs-Seymour, Kristin Uth, Christian Sieg, André P Gehring, Ivan Ahel, Franz Bracher, Benedikt M Kessler, Jonathan M Elkins, and Stefan Knapp

ACS Chem. Biol., **Just Accepted Manuscript** • DOI: 10.1021/acschembio.7b00445 • Publication Date (Web): 09 Oct 2017

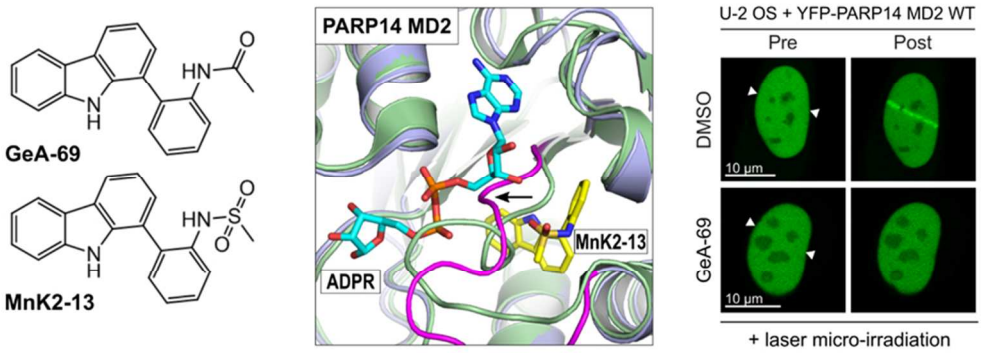

Allosteric inhibitors for the second macrodomain of PARP14 were identified. The binding mode of the lead compounds was determined using crystallographic methods. The inhibitors prevented recruitment of the PAPP14 macrodomain to DNA damage sites induced by lase irradiation.

331x124mm (72 x 72 DPI)

Discovery of a selective allosteric inhibitor targeting macrodomain 2 of poly-adenosine-diphosphate-ribose polymerase 14

Marion Schuller[1, 2], Kerstin Riedel[3], Ian Gibbs-Seymour[4], Kristin Uth[1, #], Christian Sieg[1, §], André P. Gehring[3], Ivan Ahel[4], Franz Bracher[3], Benedikt M. Kessler[2, *], Jonathan M. Elkins[1, *] & Stefan Knapp[1,5, 6, *]

[1]Structural Genomics Consortium (SGC), Nuffield Department of Clinical Medicine, University of Oxford, Oxford, OX3 7DQ, UK

[2]Target Discovery Institute (TDI), Nuffield Department of Clinical Medicine, University of Oxford, Oxford, OX3 7FZ, UK

[3]Department of Pharmacy – Center for Drug Research, Ludwig-Maximilians University of Munich, 81377 Munich, Germany

[4]Sir William Dunn School of Pathology, University of Oxford, South Parks Road, Oxford, OX1 3RE, UK

[5]Institute of Pharmaceutical Chemistry and Buchmann Institute for Molecular Life Sciences, Goethe University, 60439 Frankfurt, Germany

[6]German Cancer Network (DKTK), Frankfurt/Mainz site

[#]current address: Division of Experimental Pathology, Institute of Pathology, University of Bern, 3008 Bern, Switzerland

[§]current address: LIMES Chemical Biology Unit, Rheinische Friedrich-Wilhelms-Universität Bonn, 53121 Bonn, Germany

*corresponding authors: B.M.K. (email: benedikt.kessler@ndm.ox.ac.uk), J.M.E. (email: jon.elkins@sgc.ox.ac.uk) and S.K. (email: knapp@pharmchem.uni-frankfurt.de)

Running Title: Selective inhibition of PARP14 macrodomain 2

Keywords: small molecule inhibitor, macrodomain, ADP-ribosylation, PARP14, DNA damage, allosteric inhibition

Author Contributions:
Conceptualization of study and experiments, J.M.E. and S.K.; Design and performance of experiments, M.S.; Synthesis of GeA-69 and derivatives, K.R., A.P.G. and F.B.; Performance of laser micro-irradiation experiments, I.G.S.; Protein crystallisation and structure determination, K.U. and J.M.E.; Resources, M.S. and C.S.; Data interpretation – DNA damage experiments, I.A.; Writing – Original Draft, M.S.; Writing – Review & Editing, J.M.E., B.M.K. and S.K. with support of all other authors.

Abstract

Macrodomains are conserved protein interaction modules that can be found in all domains of life as well as in certain viruses. Macrodomains mediate recognition of sequence motifs harbouring adenosine diphosphate ribose (ADPR) modifications, thereby regulating a variety of cellular processes. Due to their role in cancer or viral pathogenesis, macrodomains have emerged as potential therapeutic targets, but the unavailability of small molecule inhibitors has hampered target validation studies so far. Here, we describe an efficient screening strategy for identification of small molecule inhibitors that displace ADPR from macrodomains. We report the discovery and characterisation of a macrodomain inhibitor, GeA-69, selectively targeting macrodomain 2 (MD2) of PARP14 with low micromolar affinity. Co-crystallisation of a GeA-69 analogue with PARP14 MD2 revealed an allosteric binding mechanism explaining its selectivity over other human macrodomains. We show that GeA-69 engages PARP14 MD2 in intact cells and prevents its localisation to sites of DNA damage.

Introduction

Protein ADP-ribosylation is catalysed by poly-ADP-ribose polymerases (PARPs) which transfer either a single adenosine diphosphate ribose (ADPR) unit (MARylation) or multiple units (PARylation) from NAD^+ onto acceptor proteins [1]. Macrodomains specifically recognise these modifications and serve therefore as "reader domains" of this posttranslational modification [2]. In addition to recognising MARylation and PARylation sites in proteins, some macrodomains control also the turnover of ADPR signalling through their ability to remove these modifications [2]. In comparison to other protein ADP-ribosylation recognising modules such as the WWE or PBZ domains, macrodomains recognise the entire ADPR moiety either directly at the protein attachment site or at the termini of poly-ADP-ribose (PAR) chains [3]. This leads to the formation of protein complexes or the recruitment to DNA lesions, i.e. sites of high PAR generation mediated by PARP1 [4–6]. Macrodomains are thus directly linked to MARylation and PARylation pathways and dysregulation of macrodomain function by overexpression or mutations have been associated with several diseases including cancer, developmental defects and neurodegeneration [2,7].

Given their pathobiological importance, macrodomains were recently suggested as potential therapeutic targets. Targeting components of ADPR signalling has already been a successful strategy for cancer therapy where PARP inhibitors have been successful in clinical trials and have been approved for treatment [8,9]. Targeting macrodomains with small molecule inhibitors may provide an attractive alternative to PARP inhibitors by disrupting ADPR signalling by a different mechanism and without the difficulties of obtaining inhibitors specific for individual PARP enzymes. So far, inhibitor development has focused on macrodomains that have enzymatic activity such as the enzyme poly(ADPR) glycohydrolase (PARG) which, similarly to PARP1, performs a critical role in DNA

damage repair [10–12]. Only recently, a chemical probe targeting PARG hydrolase activity was released which shows convincing on-target pharmacology and selectivity in contrast to early inhibitors such as rhodamine or salicylanilide based compounds [13–15].

Macrodomain inhibitor development has been hampered due to the lack of suitable high-throughput screening (HTS)-compatible biochemical assays to identify chemical starting points for drug discovery projects. Stowell *et al.* recently reported a HTS HTRF screening assay used for inhibitor discovery targeting the glycohydrolase activity of PARG [16]. This assay is, however, specific for PARG and does not enable identification of inhibitors for other macrodomains that have reader domain function.

In this work, we developed an AlphaScreen based screening strategy suitable for high-throughput screening of most human macrodomains. Using this assay, we identified a selective, allosteric and cell-active macrodomain inhibitor, GeA-69, targeting macrodomain 2 of PARP14 *in vitro* and in intact cells where it prevents its localisation to the sites of DNA damage.

Results

Identification of the PARP14 MD2 inhibitor GeA-69.

The majority of the 16 human macrodomain proteins are reader domains of protein ADP-ribosylation and only four of them show additional catalytic activity [2]. We therefore adapted an AlphaScreen (amplified luminescence proximity homogenous assay) based displacement binding assay using a peptide that was both biotinylated and mono-ADP-ribosylated together with His_6-tagged macrodomains. This strategy led to the development of an AlphaScreen assay at low peptide concentration creating an excellent signal (Figure 1A). Isothermal titration calorimetry (ITC) was used for selected macrodomains (Figure S1) in order to determine binding affinities in solution. The ITC data verified that the ADP-ribosylated peptide was recognised by macrodomains although a decrease of at least 2-fold in binding affinities to the peptide in comparison to the free ADPR monomer was observed. This decrease could be due to the method of conjugation to the peptide which resulted in a ring-opened terminal ribose unit [17], or alternatively due to the presence of the attached peptide sequence. The assay conditions were optimised for nine macrodomain proteins representing different members of the phylogenetic tree of human macrodomains. A stable assay signal was also obtained for the catalytically active macrodomains MacroD1, MacroD2 and TARG1 confirming that the ADPR imitating part was not hydrolysed. Furthermore, the consistency of the assay signal and of Z' (on average 0.85) for all of the macrodomains tested demonstrated the robustness of the assay.

Using this assay, we then performed a screen of ~48,000 small molecules against PARP14 MD2 (Figure 1A). In an initial screen, PARP14 MD2 was screened along with four other macrodomains against an in-house kinase inhibitor library of 3000 compounds at a compound concentration of 50 μM. Following this, the NDDI (NIBR Drug Discovery Incubator) compound library comprising 45,000 compounds provided by Novartis (Basel, Switzerland) was screened against PARP14 MD2 at a compound concentration of 25 μM. The rationale behind a kinase inhibitor screen was that macrodomains as binding domains of ADPR, which is structurally closely related to ATP, may show activity towards ATP-competitive kinase inhibitors or fragments. Being aware of the susceptibility of the AlphaScreen for assay interfering compounds [18], all initial hits showing more than 50 % macrodomain inhibition were validated by counter screening using a biotinylated-His_6 peptide, dose response experiments to obtain IC_{50} values, and secondary assays including biolayer interferometry (BLI) and ITC measurements.

From this screen, we identified GeA-69, which was part of the kinase inhibitor library, as initial hit for PARP14 MD2. BLI and ITC experiments verified its binding to PARP14 MD2 with a K_D of 1.4 μM and 860 nM, respectively, in a 1:1 binding stoichiometry; a closely related compound MnK2-68 (developed during an inhibitor optimisation programme) did not bind and was used as a negative control (Figure 1B - D).

GeA-69 is an allosteric inhibitor of PARP14 MD2.

To establish the binding mode of GeA-69, we first attempted to determine the co-crystal structure of PARP14 MD2 with GeA-69. Initial attempts at co-crystallisation of GeA-69 with wild-type PARP14 MD2 gave crystals that diffracted X-rays only to modest resolution. Five different surface-entropy-reduction (SER) mutants of PARP14 MD2 were prepared. In these SER constructs, up to five lysine residues on the protein surface were truncated to serine residues, to improve the likelihood of forming tighter crystal contacts [19]. Each of these mutant proteins was used in crystallisation trials with either GeA-69 or closely-related analogues. Finally, a construct of the PARP14 $MD2_{K1048S, K1154S, K1158S, K1162S}$ mutant gave a crystal diffracting to 1.6 Å resolution (Table 1) in complex with compound MnK2-13 (Figure 2A). MnK2-13 is the methanesulfonamide analogue of the acetamide GeA-69 and binds to PARP14 MD2 with a K_D of 2.1 μM (Figure S2A).

Compound MnK2-13 was well resolved in the electron density (Figure S2B). Surprisingly MnK2-13 did not occupy the ADPR binding site but was deeply buried within the macrodomain with no contact with the solvent phase (Figure 2A). Ligand binding was stabilised by hydrophobic and hydrogen bonding interactions to the protein (Figure 2B). The planar carbazole itself was bound in a hydrophobic pocket with several hydrophobic interactions including the T-shaped π-π interaction with ring C and F1129 and with an additional hydrogen bond of the NH of the carbazole to the proline carbonyl of P1130. The benzene ring of MnK2-13 was surrounded by hydrophobic residues including F1182, L1171 and F1169. The sulfonamide moiety of MnK2-13 formed several hydrogen bonds to the macrodomain including to the amide of I1132 and the primary carboxamide of the N1178 side chain. Furthermore, the NH of the sulfonamide group was involved in a complex with a water molecule together with the N1178 carbonyl group and K1141. Superimposition of the ADPR-bound macrodomain structure (PDB 3Q71) and the MnK2-13-bound structure furthermore showed that F1144 was pushed aside by the carbazole of the inhibitor. Ring A of the carbazole may therefore be crucial for enabling the binding of the inhibitor to the protein.

MnK2-13 bound adjacent to but not in the ADPR binding site as would have been expected based on its carbazole scaffold that was used for the development of ATP mimetic inhibitors [20]. The structure superimposition revealed that upon inhibitor binding a loop from P1130 to P1140 was pushed into the ADPR binding site displacing the bound ADPR (Figure 2C), and a portion of this loop consisting of residues G1133-G1135 has weaker electron density and may thus be present in multiple conformations. ITC competition experiments confirmed GeA-69 as an allosteric inhibitor of PARP14 MD2 able to prevent ADPR binding to the macrodomain. In the presence of 80 μM GeA-69, binding of ADPR to the macrodomain was not detected while in absence of the inhibitor recognition of the ADPR with a K_D of 7.8 μM was measured (Figure 2C).

GeA-69 is a highly selective macrodomain inhibitor.

To assess GeA-69 selectivity over the other human macrodomain family members, we tested the inhibitor on eleven other representative human macrodomain proteins either by the macrodomain AlphaScreen assay at a compound concentration of 200 μM, by BLI at a compound concentration of 50 μM or by ITC at a compound concentration of 30 μM (Figure 3A, S4). Binding was only detected to PARP14 MD2 proving the very high target selectivity of GeA-69 over the macrodomain family. Although the macrodomain fold is highly conserved, at the amino acid level sequence divergence is high, and structural and sequence comparison revealed a number of differences around the binding site that provide a rationale for the excellent selectivity of GeA-69 (Figure 3B, S5, S6). Since GeA-69 was part of a kinase inhibitor library, originally synthesised in a programme aimed at the optimisation of the activities of the alkaloid annomontine [21,22], the internal database was searched for experimental thermal shift assay data of kinases that were screened against this compound. A number of 46 kinases representing different branches of the phylogenetic kinase tree were screened (Figure S7), none of them showing any significant stability shifts and thus no binding affinity for this inhibitor. Further *in vitro* profiling showed that GeA-69 exhibited, despite its allosteric binding mode, fast on/fast off kinetics when binding to PARP14 MD2, with a mean dissociation rate constant of 2.4×10^{-2} s^{-1} resulting in a half-life of binding ($t_{1/2}$, residence time) of 42 seconds (Figure 3C). Performance of parallel artificial membrane permeability assays (PAMPA) showed that GeA-69 was highly cell permeable with a $logP_e$ of -3.5 over three representative pH values (4.0, 6.8, 8.0) (Figure 3D). Finally, metabolic activity assays showed that GeA-69 has only moderate cytotoxicity with an EC_{50} of ~50 μM on different cell lines tested (HeLa, HEK293 and U-2 OS) (Figure 3E). Altogether, GeA-69 demonstrated a biochemical profile to warrant the evaluation of cell-based activities.

GeA-69 engages PARP14 MD2 in intact cells.

Since PARP14 macrodomains have been reported to localise to sites of DNA damage [23], we tested the ability of GeA-69 to interfere with PARP14 MD2 recruitment to laser-induced DNA damage sites. In order to confirm that PARP14 MD2 is actively recruited to DNA damage sites, BrdU sensitised U-2 OS cells were transfected with YFP-PARP14 MD2 and subjected to laser micro-irradiation coupled to live-cell imaging. We observed that PARP14 MD2 is recruited to these DNA lesions within seconds after induction of DNA damage, while the corresponding ADPR binding deficient PARP14 $MD2_{G1044E}$ mutant was not able to localise to these sites (Figure 4A, S8). Furthermore, PARP14 MD2 recruitment depends on both the presence and activity of PARP1. In the absence of PARP1, in $PARP1^{-/-}$ cells, and after inhibition of PARP1 catalytic activity using the PARP inhibitor Olaparib, recruitment of the macrodomain could not be detected in comparison to the corresponding controls (Figure 4B, C). Finally, we evaluated if GeA-69 could interfere with the PARP14 MD2 recruitment and observed that pre-treatment of U-2 OS cells with GeA-69 for 2 hrs affected PARP14 MD2 re-localisation in this set-up. The macrodomain recruitment was significantly decreased in cells pre-treated with 50 μM GeA-69 and completely prevented in cells exposed to 250 μM GeA-69. As

expected, the negative control MnK2-68 did not interfere with PARP14 MD2 recruitment and further, GeA-69 did not affect the recruitment of an alternative macrodomain containing protein, YFP-ALC1. Although a high inhibitor concentration had to be applied to completely prevent PARP14 MD2 recruitment to DNA damage sites, these experiments proved that GeA-69 engages PARP14 MD2 in intact cells.

Discussion

Although representative members of human, viral or bacterial macrodomains have so far been well studied regarding their molecular structure, substrate recognition and *in vitro* biochemical activity, very limited data is available on their *in vivo* characterisation which would provide a detailed understanding of their (patho-)physiological functions. Those studies would be aided by inhibitors that specifically target members of the macrodomain family. Great progress has been made on the development of cell-active and potent inhibitors of the catalytic activity of PARPs and of the hydrolase PARG, however, to the best of our knowledge inhibitors of other macrodomains have not been reported so far. To address this challenge, we have developed an AlphaScreen based assay suitable for high-throughput screening of several human (catalytically active or inactive) macrodomains. We anticipate that this assay is also applicable for screening most non-human macrodomains that bind ADPR. Using this assay, we identified a small molecule inhibitor, GeA-69, targeting PARP14 MD2 with low micromolar affinity. GeA-69 is a carbazole-based compound with an acetylaminophenyl substituent attached to ring A. This, and very few related compounds, e.g. the methanesulfonamide analogue MnK2-13 showed significant inhibition of PARP14 MD2. An allosteric binding mode was proven by an X-ray crystal structure analysis. A detailed structure-activity-relationship (SAR) study showing our attempts to improve the scaffold and potency of this inhibitor will be published elsewhere.

PARP14 is described as pro-survival protein and is associated with the development of inflammatory diseases and various types of cancer including B-cell lymphoma and hepatocellular carcinoma [24–26]. PARP14 has therefore emerged as a therapeutic target and there are concurrent approaches that focus on the development of inhibitors targeting its catalytic PARP domain [27–29]. PARP domain inhibitors are however challenging to optimise in regard to their selectivity over PARP1. Targeting PARP14 macrodomains is an alternative strategy to interfere with PARP14 recruitment to ADP-ribosylated target sites through its macrodomains and consequently prevent MARylation of target proteins by its catalytic domain. GeA-69 shows good ligand efficiency and excellent selectivity over other human macrodomains, obviously as a consequence of its allosteric binding mode. More importantly, GeA-69 is cell-active and prevents PARP14 MD2 recruitment to DNA damage sites. To what extent these laser micro-irradiation assays already reflect endogenous PARP14 activity in DNA damage repair mechanisms is under current investigation.

Figures:

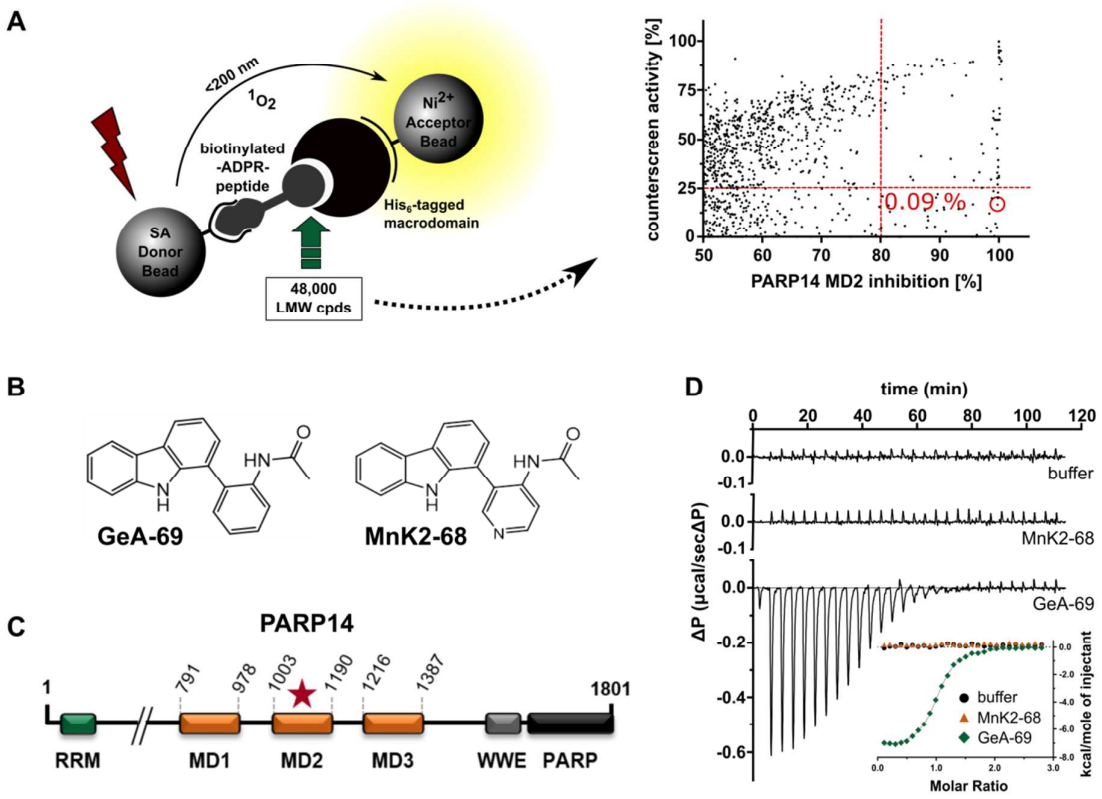

Figure 1. ***Structure and identification of the PARP14 MD2 inhibitor GeA-69.*** **(A)** Performance of a 48,000 compound screen against PARP14 MD2 by AlphaScreen. The graph represents the screening of two libraries and displays the AlphaScreen activity of 961 compounds that showed more than 50 % macrodomain inhibition. 0.09 % of the 48,000 compounds showed more than 80 % inhibition of the macrodomain and less than 25 % activity in the counterscreen (red lines). GeA-69 is highlighted with a red circle. **(B)** Molecular structure of the macrodomain inhibitor GeA-69 and its inactive analogue MnK2-68. **(C)** Schematic representation of the PARP14 domain architecture. Residue numbers refer to the human PARP14 (NCBI ref: NP_060024). The macrodomain targeted by GeA-69 is highlighted with a red star. **(D)** Isothermal titration calorimetry (ITC) confirmed binding of GeA-69 to PARP14 MD2 with a K_D of 860 nM. Raw injection heats are shown for a blank titration of PARP14 MD2 into buffer (top), and titrations of PARP14 MD2 into solutions of the inactive analogue MnK2-68 (middle) and the active compound GeA-69 (bottom). The inset shows normalized binding enthalpies corrected for the heat of dilution as a function of binding site saturation (symbols as indicated in the inset). Solid lines represent a nonlinear least squares fit using a single-site binding model.

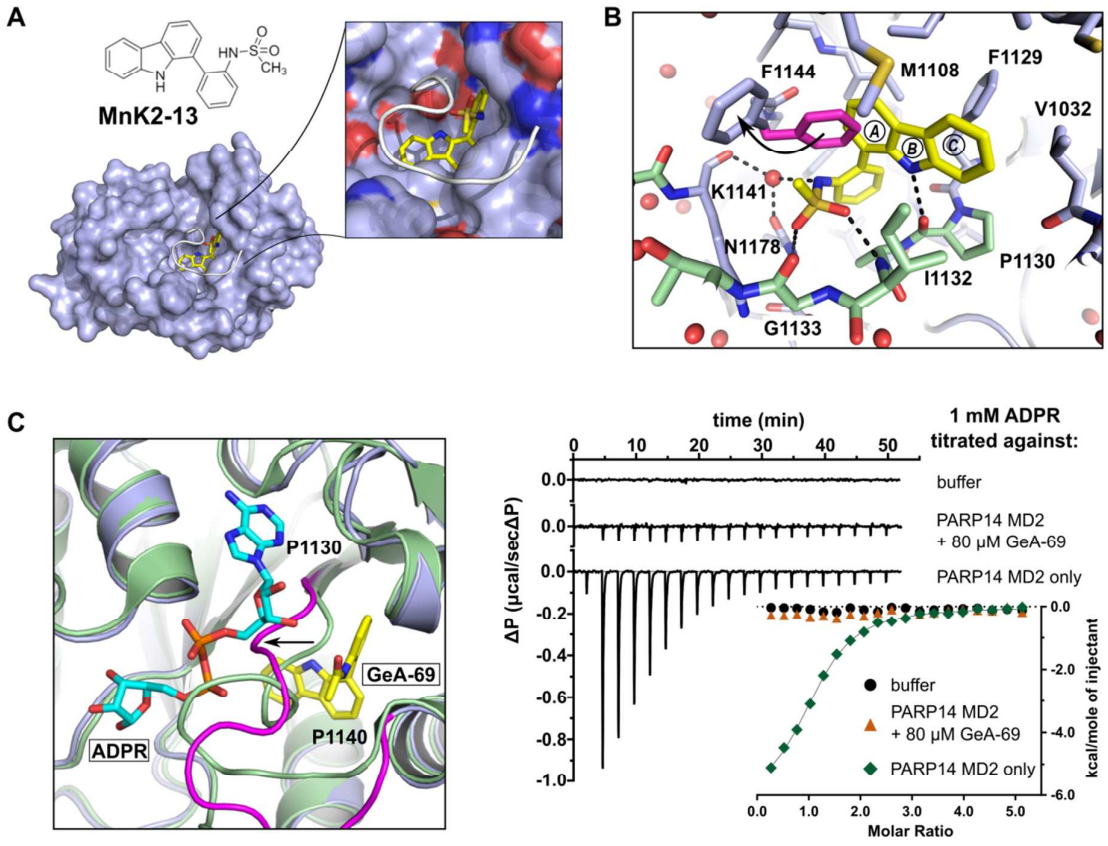

Figure 2. ***Crystal structure of PARP14 MD2 in complex with MnK2-13 reveals an allosteric binding mode.*** **(A)** Surface representation of PARP14 MD2 in complex with the macrodomain active GeA-69 analogue MnK2-13. The macrodomain inhibitor (atom-coloured sticks) is deeply bound within the macrodomain. The solvent accessible surface of residues 1234-1234 (white loop) was removed to visualise the inhibitor. **(B)** The binding site of MnK2-13 in PARP14 MD2. Residues involved in direct contacts with the inhibitor are shown in atom-coloured sticks. Hydrogen bonds between ligand and protein or structural waters are indicated by dotted lines. Superimposition of the ADPR bound macrodomain structure (PDB 3Q71) and inhibitor bound macrodomain structure shows that F1144 (magenta) is pushed aside by the carbazole ring system of MnK2-13 (arrow). The part of the loop (P1130-P1140) that is rearranged by comparison to the ADPR bound structure is shown in green. **(C)** GeA-69 is an allosteric inhibitor of ADPR binding to PARP14 MD2. **(Left)** GeA-69 was docked into PARP14 MD2 using the PARP14 MD2-MnK2-13 co-crystal structure as template (PDB 5O2D). Superimposition of the resulting docking structure with the ADPR-bound macrodomain structure (PDB 3Q71, green) revealed GeA-69 as allosteric inhibitor. Binding of GeA-69 (or the macrodomain active analogue MnK2-13) to the macrodomain results in movement of the loop P1130-P1140 (highlighted in magenta) into the ADPR binding site displacing the bound ADPR. **(Right)** ITC experiments confirmed GeA-69 as an inhibitor of ADPR binding to PARP14 MD2. Raw injection

heats are shown resulting from titration of a 1 mM ADPR solution into the cell containing either buffer (top) or 40 μM PARP14 MD2 only (bottom) or 40 μM PARP14 MD2 in presence of 80 μM GeA-69 (middle). Only in absence of the inhibitor, the expected K_D for ADPR of 7.8 μM was observed.

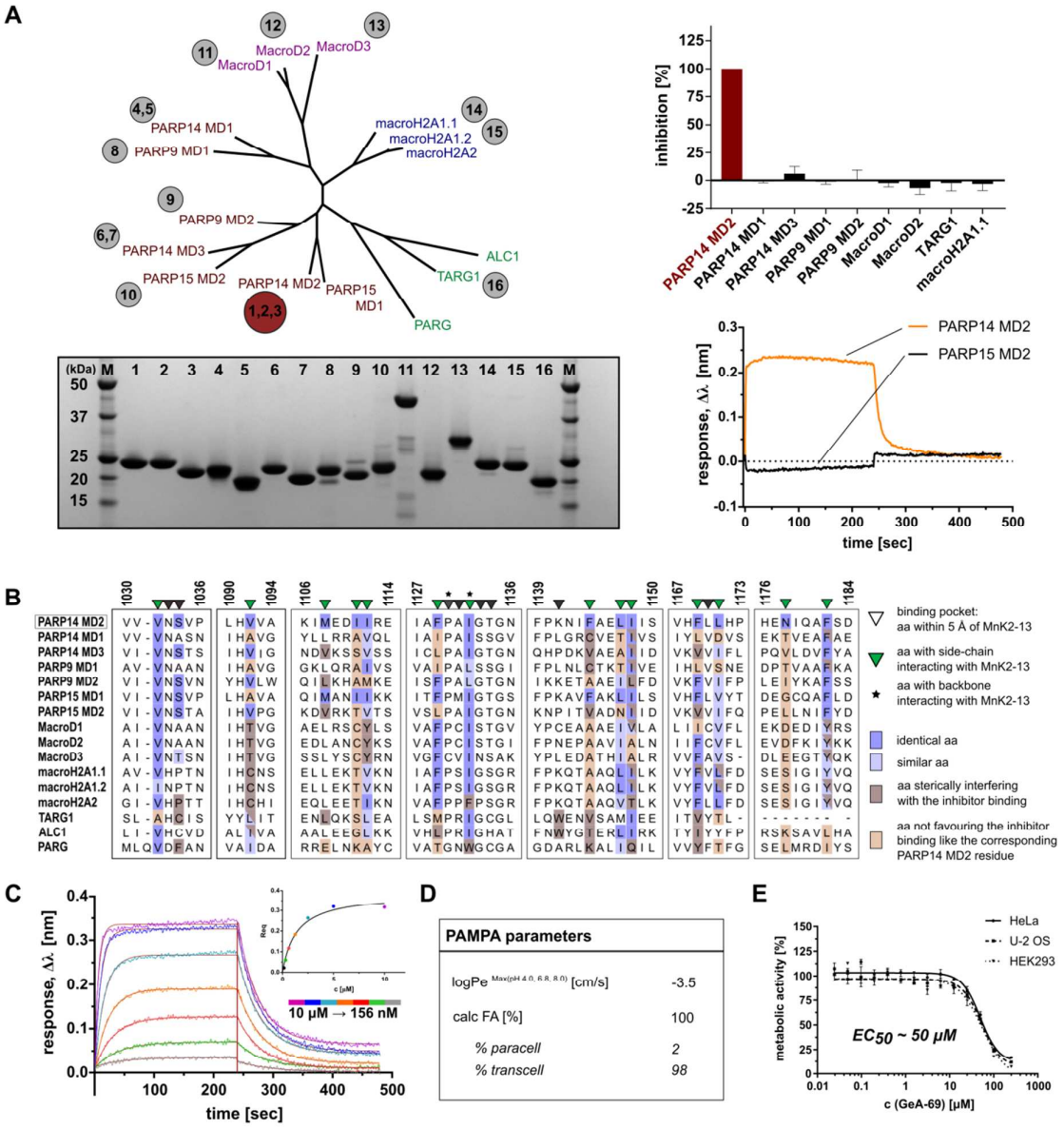

Figure 3. ***GeA-69 is a selective and highly cell permeable macrodomain inhibitor.*** **(A)** GeA-69 shows target selectivity over human macrodomain family members. Selectivity was assessed for 12 out of 16 human macrodomains (shown by circles) by the macrodomain AlphaScreen assay at a compound concentration of 200 µM (top right) or by biolayer interferometry (BLI) at a compound concentration of 50 µM (bottom right). Binding was only detected with PARP14 MD2 (red circle). The numbers in the circles correspond to macrodomains shown on SDS-PAGE (bottom left). PARP14 MD1, 2 and 3 proteins were prepared with different tags. Details are provided in Figure S3. **(B)** Multiple sequence alignment of human macrodomains confirming no other human macrodomain has conserved all the residues that bind MnK2-13 and therefore also GeA-69. Residues of PARP14 MD2

involved in MnK2-13 interaction are highlighted in green, numbers on top of the alignment refer to the human PARP14 sequence. Box colour legend: (blue) identical amino acid, (light blue) similar amino acid, (brown) amino acid likely to sterically interfere with inhibitor binding, (light brown) amino acid not favouring the inhibitor binding like the corresponding PARP14 MD2 residue based on its physicochemical properties. **(C)** Binding kinetics of GeA-69 to PARP14 MD2. The BLI sensorgram shows the kinetics of GeA-69 association and dissociation to PARP14 MD2. The inhibitor concentration range and steady state analysis are shown next to the traces. Mean k_a is 1.35×10^4 $M^{-1}s^{-1}$ while the mean k_d is 2.4×10^{-2} s^{-1} resulting in a half-life of binding ($t_{1/2}$, residence time) of 42 seconds. **(D)** GeA-69 is highly cell permeable. Cell permeability was assessed by PAMPA (parallel artificial permeability assay) performance. The highest effective permeability (logPe) of -3.5 is identical over the three representative pH values tested. The fraction of absorbed drug (FA) was calculated to 100 % with 2 % passing paracellular and 98 % transcellular over the membrane. Active transport mechanisms are not considered in this model. **(E)** GeA-69 shows moderate cytotoxicity. HeLa, U-2 OS and HEK293 cells were incubated for 72 h in the presence of different GeA-69 concentrations (25 nM - 250 µM) and cell viability was measured using the AlamarBlue™ reagent. EC_{50} values were calculated from three independent experiments (EC_{50_HeLa} = (58 ± 3.9) µM, $EC_{50\_U\text{-}2\ OS}$ = (52 ± 1.1) µM, EC_{50_HEK293} = (54 ± 2.2) µM. Results are expressed as mean ± SEM, n = 3).

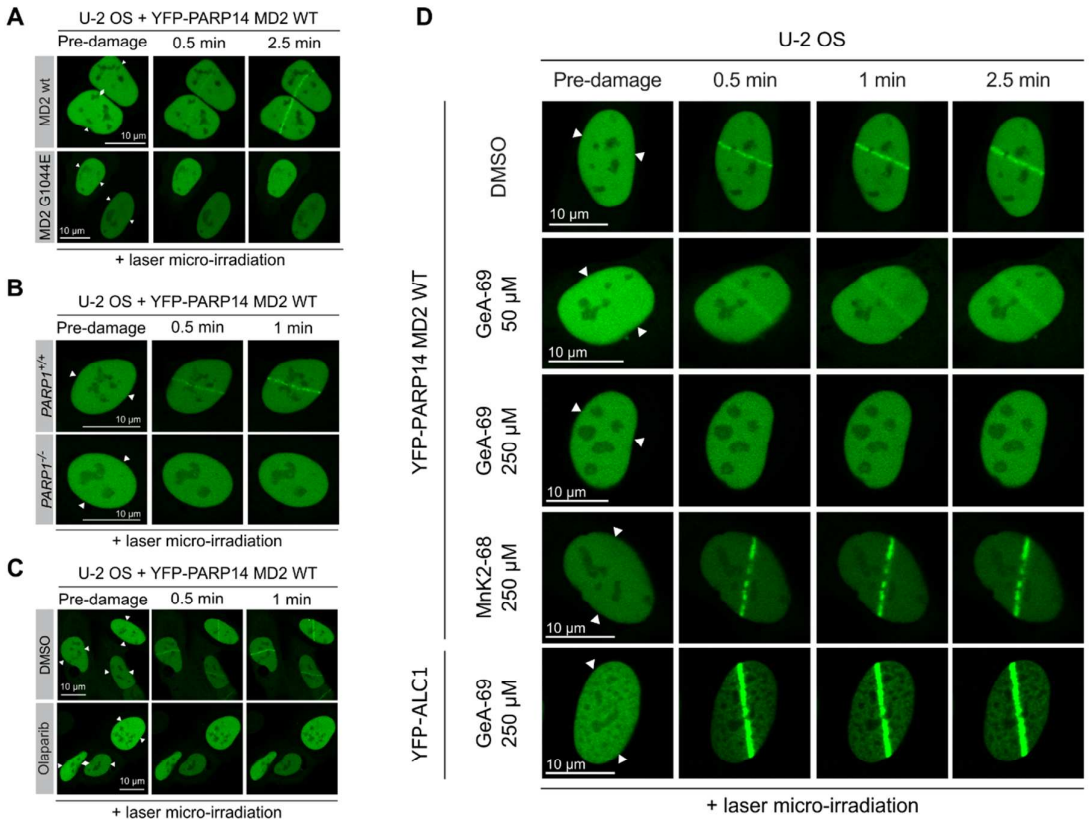

Figure 4. ***GeA-69 engages PARP14 MD2 and prevents localisation to the sites of DNA damage.***

(A) PARP14 MD2 wild-type is recruited to sites of laser-induced DNA damage in contrast to the corresponding ADPR binding deficient mutant G1044E. U-2 OS cells were transfected with YFP-PARP14 MD2 wt or G1044E mutant, subjected to laser micro-irradiation (white arrows) and imaged at the indicated times. **(B)** PARP14 MD2 recruitment depends on the presence of PARP1. U-2 OS/*PARP1*$^{+/+}$ and U-2 OS/*PARP1*$^{-/-}$ cells were transfected with YFP-PARP14 MD2 wt, subjected to laser micro-irradiation and imaged at the indicated times. **(C)** PARP14 MD2 recruitment depends on the activity of PARP1. U-2 OS cells transiently expressing YFP-PARP14 MD2 wt were pre-treated for 1 hour with DMSO or with 10 µM of the PARP1 inhibitor Olaparib, subjected to laser micro-irradiation and imaged at the indicated times. **(D)** GeA-69 prevents recruitment of PARP14 MD2 to sites of laser-induced DNA damage. U-2 OS cells transiently expressing YFP-PARP14 MD2 or full-length YFP-ALC1 were pre-treated with DMSO, GeA-69 or the negative control inhibitor MnK2-68, subjected to laser micro-irradiation and imaged at the indicated times.

Table 1. ***Data collection and refinement statistics.***

PDB ID	5O2D
Space group	*C*2
No. of molecules in the asymmetric unit	1
Unit cell dimensions *a*, *b*, *c* (Å), β (°)	131.4, 35.7, 37.1, 94.8
Data collection	
Resolution range (Å)[a]	27.65-1.60 (1.63-1.60)
Unique observations[a]	22712 (1036)
Average multiplicity[a]	3.8 (2.7)
Completeness (%)[a]	98.9 (90.7)
R_{merge}[a]	0.05 (0.22)
Mean $(I)/\sigma(I)$[a]	12.2 (3.6)
Mean CC(1/2)	0.998 (0.925)
Refinement	
R-value, R_{free} (%)	13.2, 17.4
r.m.s. deviation from ideal bond length (Å)	0.011
r.m.s. deviation from ideal bond angle (°)	1.48

[a] Values within parentheses refer to the highest resolution shell.

Experimental Procedures

Materials and plasmids

Bacterial expression constructs encoding PARP14 MD1 (G789–K979), PARP14 MD2 (A994–N1191) and PARP14 MD3 (F1208–G1388) were a kind gift from Herwig Schüler [30]. Full-length PARP14 cDNA was obtained from Genecopoeia. The macrodomain AlphaScreen™ peptide was synthesized by Cambridge Peptides (Birmingham, UK) and has the following sequence: ARTK(Bio)QTARK(Aoa-RADP)S (M.W.: 1986.8; purity: 92 %, peptide code: 19254). *D*-biotin and adenosine 5′-diphosphoribose sodium salt (purity: 95 %) were purchased from Sigma Aldrich.

Macrodomain AlphaScreen™ assay

Assays were performed with minor modifications from the manufacturer's protocol (PerkinElmer). All reagents were diluted in buffer containing 25 mM HEPES (pH 7.4), 100 mM NaCl, 0.5 mM TCEP, 0.1 % bovine serum albumin and 0.05 % CHAPS and allowed to equilibrate to room temperature before addition to plates. The assays were run in 20 µL volumes in low-volume 384-well plates (ProxiPlate™-384 Plus, PerkinElmer, USA) at RT. To determine ideal assay concentrations of the corresponding macrodomain protein and peptide (a biotinylated and ADP-ribosylated 11 residue sequence, Figure S1A), 4 µL volumes of peptide (0-16 µM; final assay concentration: 0-3.2 µM) were incubated with 4 µL volumes of His_6-tagged macrodomain protein (0-16 µM; final assay concentration: 0-3.2 µM) in 4 µL buffer for 30 min at RT in foil-sealed plates. For compound screening, 12 µL of a solution containing 25 nM peptide and 400 nM His_6-tagged PARP14 MD2 protein in assay buffer were incubated with 50 nL or 100 nL compound solution (10 mM; final assay concentration: 25 µM or 50 µM) for 30 min at RT in foil-sealed plates. Then, 8 µL of streptavidin-coated donor beads (7 µg/ml) and nickel chelate acceptor beads (7 µg/ml) (Perkin Elmer AlphaScreen™ Histidine (Nickel Chelate) Detection Kit) were added under low light conditions and plates were incubated for 60 min at RT protected from light. Plates were read on a PHERAstar FS plate reader (BMG Labtech, Germany) using an AlphaScreen™ 680 excitation/570 emission filter set. Alternatively for counter screening of the compounds, 12 µL of 75 nM biotinylated and hexahistidine-tagged linker peptide (PerkinElmer) was added to 50 nL or 100 nL of the compounds (10 mM) and plates were processed as described above.

Isothermal titration calorimetry (ITC)

Binding experiments were carried out on a VP-ITC microcalorimeter (MicroCal). All experiments were performed in 50 mM HEPES (pH 7.4), 300 mM NaCl, 5 % glycerol, 0.5 mM TCEP at 12 °C, a reference power of 12 µCal/sec and a stirring speed of 307 rpm. The titrations were conducted using an initial injection of 2 µL followed by 28 identical injections of 10 µL with duration of 4 sec (per injection) and a spacing of 240 sec between injections. Competition experiments were performed on an iTC200 instrument (MicroCal) at 20 °C, a reference power of 12 µCal/sec and a stirring speed of 1000 rpm. Following an initial injection of 0.2 µL, 20 identical injections of 2 µL were run with a

duration of 4 sec (per injection) and a spacing of 150 sec between injections. Data analysis was carried out using Origin software with the MicroCal plugin. Thermodynamic parameters were calculated using $\Delta G = \Delta H - T\Delta S = -RT\ln K_B$, where ΔG, ΔH, and ΔS are the changes in free energy, enthalpy, and entropy of binding, respectively. In all cases, a single binding site model was employed.

Biolayer interferometry (BLI)

Kinetic ligand-binding measurements were performed using an Octet RED384 BLI instrument (fortéBio). Superstreptavidin (SSA) biosensors were loaded with biotinylated macrodomain protein and equilibrated for 120 sec in assay buffer (25 mM HEPES (pH 7.4), 100 mM NaCl, 0.01 % Tween 20). Association and dissociation were monitored for 240 sec each in assay buffer at 25 °C. GeA-69 was prepared as seven 1:1 serial dilutions starting from 10 µM. Binding to the reference sensors (no protein attached) was subtracted before calculations and data was processed using the fortéBio analysis software provided by the manufacturer.

Protein crystallisation and data collection

Surface entropy reduction mutations were introduced into PARP14 MD2 (A994–N1191) by the overlapping PCR method. Several mutants were prepared of which PARP14 $MD2_{SER3}$ with K1048S, K1154S, K1158S, and K1162S mutations could be crystallised with MnK2-13. For protein crystallisation, purified PARP14 $MD2_{SER3}$ was buffer-exchanged into 20 mM HEPES (pH 7.4), 500 mM NaCl, 5 % glycerol, 0.5 mM TCEP, and concentrated to 16 mg/ml, using 10 kDa MWCO centrifugal concentrators (Millipore). MnK2-13 inhibitor dissolved to 50 mM in DMSO was added to a final concentration of 1.0 mM (2 % DMSO) and incubated on ice for approximately 30 min. The sample was centrifuged at 14,000 rpm for 10 min at 4 °C prior to setting up 150 nL volume sitting drops at three ratios (2:1, 1:1 or 1:2 protein-inhibitor complex to crystallisation solution). Drops were equilibrated at two temperatures (4 °C or 20 °C). A crystal was obtained with a 1:2 ratio of protein to a crystallisation solution consisting of 0.8 M sodium phosphate monobasic, 0.8 M potassium phosphate dibasic, 0.1 M HEPES pH 7.5, and was cryoprotected in mother liquor supplemented with 25 % ethylene glycol before flash-freezing in liquid nitrogen for data collection. Diffraction data were collected at the Diamond Light Source beamline I02.

Structure solution and refinement

The diffraction data was processed using MOSFLM [31] and AIMLESS [32] (Table 1). The structure was solved by molecular replacement using PHASER [33] and a published structure of PARP14 MD2 (PDB ID 3Q71) as a search model. There was one molecule of PARP14 MD2 in the asymmetric unit. Coot [34] and REFMAC5 [35] were used for building the model and refinement. MOLPROBITY [36] was used for model validation and analysis.

Synthesis of GeA-69, MnK2-13 and MnK2-68

GeA-69, *N*-[3-(9*H*-carbazol-1-yl)pyridin-4-yl]acetamide, was prepared from known [37] 1-bromocarbazole by a Suzuki cross-coupling procedure as follows: 74 mg (0.30 mmol) 1-bromo-9*H*-carbazole, 61 mg (0.31 mmol) 2-acetamidophenylboronic acid, and 39 mg (0.034 mmol) $Pd(Ph_3P)_4$

were placed in a microwave vial under nitrogen atmosphere. A mixture of 3 mL 1,2-dimethoxyethane und 2 mL ethanol, previously degassed by purging with for 10 min with nitrogen, was added. The suspension was stirred for 10 min at room temperature. Then 1.0 mL 2 M degassed sodium carbonate solution was added. The reaction was conducted for 10 min under microwave irradiation at 70 °C, 150 Watt and a maximum pressure of 6 bar. After cooling of the reaction mixture in an ice bath, water (50 mL) was added, followed by extraction with diethyl ether (3 x 40 mL). The combined organic layers were dried over sodium sulfate and concentrated in vacuum. The residue was purified by flash column chromatography (dichloromethane/ethyl acetate 2:1). Yield: 55 mg (0.18 mmol / 60 %) light grey solid. Melting point: 173-175 °C. ^{1}H-NMR (500 MHz, CD_2Cl_2): δ (ppm) = 8.31 (br s, 1H, 9-NH), 8.26 (d, J = 8.2 Hz, 1H, 6´-H), 8.15 (dd, J = 6.1 Hz, 2.8 Hz, 1H, 4-H), 8.12 (d, J = 7.7 Hz, 1H, 5-H), 7.47 – 7.41 (m, 2H, 4´-H, 5´-H), 7.41 – 7.39 (m, 2H, 7-H, 8-H), 7.37 – 7.34 (m, 2H, 2-H, 3-H), 7.29 (d, J = 6.8 Hz, 1H, 3´-H), 7.25 (ddd, J = 8.0 Hz, 7.8 Hz, 2.6 Hz, 1H, 6-H), 7.11 (br s, 1H, 1´-NH), 1.76 (s, 3H, CH_3). ^{13}C-NMR (100 MHz, CD_2Cl_2): δ (ppm) = 169.2 (C=O), 140.1 (C-8a), 138.2 (C-9a), 136.1 (C-1´), 131.0 (C-5´), 129.4 (C-2´), 129.2 (C-4´), 127.0 (C2), 126.7 (C-7), 125.2 (C-3´), 124.1 (C-4a), 123.6 (C-4b), 122.9 (C-6´), 120.9 (C-1), 120.8 (C-5), 120.7 (C-4), 120.2 (C-3), 120.1 (C-6), 111.3 (C-8), 24.6 (CH_3).

Methanesulfonamide analogue MnK2-13 was prepared in a similar manner, starting from 1-bromocarbazole, by Suzuki cross-coupling with 2-aminophenylboronic acid, followed by N-sulfonylation with methanesulfonyl chloride. For details see Supplemental Information. The synthesis of the inactive analogue MnK2-68, a novel approach, including SEM-protection of 1-bromocarbazole, Masuda borylation at C-1, Suzuki cross-coupling with 4-amino-3-bromopyridine, and subsequent N-acetylation and SEM deprotection was worked out. For details, see Supplemental Information.

Laser micro-irradiation assays

Laser micro-irradiation was performed as described previously [38]. U-2 OS wild-type or *PARP1*$^{-/-}$ cells were pre-sensitised for 24 h with 10 μM BrdU (Sigma), then the media was changed to Live Cell Imaging Solution (Thermo Fisher) before laser micro-irradiation and imaging. Laser micro-irradiation was performed on an Olympus Fluoview FV1200 confocal microscope equipped an inverted IX83 motorised stage with a 37 ºC humidified chamber and 60x/1.40 oil UPlanSApo objective and 405 nm laser.

Acknowledgements:

The authors are grateful for financial support by the SGC, a registered charity (number 1097737) that receives funds from AbbVie, Bayer Pharma AG, Boehringer Ingelheim, Canada Foundation for Innovation, Eshelman Institute for Innovation, Genome Canada through Ontario Genomics Institute, Innovative Medicines Initiative (EU/EFPIA) [ULTRA-DD grant no. 115766], Janssen, Merck & Co., Novartis Pharma AG, Ontario Ministry of Economic Development and Innovation, Pfizer, São Paulo Research Foundation-FAPESP, Takeda, the Centre of Excellence (CEF) Macromolecular Complexes

at Frankfurt University, and the Wellcome Trust. Funding for M.S. was also provided by the EPSRC (award reference: 1368548) and Novartis Pharma AG through the Systems Approaches to Biomedical Sciences – Industrial Doctoral Centre (SABS-IDC) programme of the University of Oxford.
We very much would like to thank Novartis Institutes for BioMedical Research (Basel) for providing the resources for the macrodomain high-throughput screen and are grateful for support and helpful advice in HTS performance and data analysis provided by J. Trappe and team members (NIBR, Basel). Furthermore, we would like to thank S. Jacob, C. Scheufler and H. Widmer (NIBR, Basel) for supporting the project. We thank N. Domage (NIBR, Basel) for generating the PAMPA data. We are grateful to O. Fedorov and team members (SGC, Oxford) for assistance with the macrodomain assay development. We thank Diamond Light Source for access to the beamline I02 for data collection and processing.

Supporting information comprising additional experimental data methods and figures is available online: This material is available free of charge via the internet at http://pubs.acs.org.

References

(1) Perina, D., Mikoč, A., Ahel, J., Ćetković, H., Žaja, R., and Ahel, I. (2014) Distribution of protein poly(ADP-ribosyl)ation systems across all domains of life. *DNA Repair (Amst). 23*, 4–16.

(2) Rack, J. G. M., Perina, D., and Ahel, I. (2016) Macrodomains: Structure, Function, Evolution, and Catalytic Activities. *Annu. Rev. Biochem. 85*, 431–454.

(3) Barkauskaite, E., Jankevicius, G., Ladurner, A. G., Ahel, I., and Timinszky, G. (2013) The recognition and removal of cellular poly(ADP-ribose) signals. *FEBS J. 280*, 3491–3507.

(4) Feijs, K. L. H., Forst, A. H., Verheugd, P., and Lüscher, B. (2013) Macrodomain-containing proteins: regulating new intracellular functions of mono(ADP-ribosyl)ation. *Nat. Rev. Mol. Cell Biol. 14*, 443–51.

(5) Tallis, M., Morra, R., Barkauskaite, E., and Ahel, I. (2014) Poly(ADP-ribosyl)ation in regulation of chromatin structure and the DNA damage response. *Chromosoma 123*, 79–90.

(6) Hottiger, M. O. (2015) Nuclear ADP-Ribosylation and Its Role in Chromatin Plasticity, Cell Differentiation, and Epigenetics. *Annu. Rev. Biochem. 84*, 227–63.

(7) Han, W., Li, X., and Fu, X. (2011) The macro domain protein family: structure, functions, and their potential therapeutic implications. *Mutat. Res. 727*, 86–103.

(8) Sonnenblick, A., de Azambuja, E., Azim, H. A., and Piccart, M. (2014) An update on PARP inhibitors—moving to the adjuvant setting. *Nat. Rev. Clin. Oncol. 12*, 27–41.

(9) Lord, C. J., and Ashworth, A. (2017) PARP inhibitors: Synthethic lethality in the clinic. *Science 355*, 1152–1158.

(10) Slade, D., Dunstan, M. S., Barkauskaite, E., Weston, R., Lafite, P., Dixon, N., Ahel, M., Leys, D., and Ahel, I. (2011) The structure and catalytic mechanism of a poly(ADP-ribose) glycohydrolase. *Nature 477*, 616–20.

(11) Mortusewicz, O., Fouquerel, E., Amé, J. C., Leonhardt, H., and Schreiber, V. (2011) PARG is recruited to DNA damage sites through poly(ADP-ribose)- and PCNA-dependent mechanisms. *Nucleic Acids Res. 39*, 5045–5056.

(12) Fisher, A. E. O., Hochegger, H., Takeda, S., and Caldecott, K. W. (2007) Poly(ADP-ribose) polymerase 1 accelerates single-strand break repair in concert with poly(ADP-ribose) glycohydrolase. *Mol. Cell. Biol. 27*, 5597–5605.

(13) James, D. I., Smith, K. M., Jordan, A. M., Fairweather, E. E., Griffiths, L. A., Hamilton, N. S., Hitchin, J. R., Hutton, C. P., Jones, S., Kelly, P., McGonagle, A. E., Small, H., Stowell, A. I. J., Tucker, J., Waddell, I. D., Waszkowycz, B., and Ogilvie, D. J. (2016) First-in-class chemical probes against poly(ADP-ribose) glycohydrolase (PARG) inhibit DNA repair with differential pharmacology to olaparib. *ACS Chem. Biol. 11*, 3179–3190.

(14) Finch, K. E., Knezevic, C. E., Nottbohm, A. C., Partlow, K. C., and Hergenrother, P. J. (2012) Selective small molecule inhibition of poly(ADP-ribose) glycohydrolase (PARG). *ACS Chem. Biol. 7*, 563–570.

(15) Steffen, J. D., Coyle, D. L., Damodaran, K., Beroza, P., and Jacobson, M. K. (2011) Discovery and structure-activity relationships of modified salicylanilides as cell permeable inhibitors of poly(ADP-ribose) glycohydrolase (PARG). *J. Med. Chem. 54*, 5403–5413.

(16) Stowell, A. I. J., James, D. I., Waddell, I. D., Bennett, N., Truman, C., Hardern, I. M., and Ogilvie, D. J. (2016) A high-throughput screening-compatible homogeneous time-resolved fluorescence assay measuring the glycohydrolase activity of human poly(ADP-ribose) glycohydrolase. *Anal. Biochem. 503*, 58–64.

(17) Moyle, P. M., and Muir, T. W. (2010) Method for the synthesis of mono-ADP-ribose conjugated peptides. *J. Am. Chem. Soc. 132*, 15878–15880.

(18) Baell, J. B., and Holloway, G. A. (2010) New substructure filters for removal of pan assay interference compounds (PAINS) from screening libraries and for their exclusion in bioassays. *J. Med. Chem. 53*, 2719–2740.

(19) Longenecker, K. L., Garrard, S. M., Sheffield, P. J., and Derewenda, Z. S. (2001) Protein crystallization by rational mutagenesis of surface residues: Lys to Ala mutations promote crystallization of RhoGDI. *Acta Crystallogr. Sect. D: Biol. Crystallogr. 57*, 679–688.

(20) Watterson, S. H., De Lucca, G. V., Shi, Q., Langevine, C. M., Liu, Q., Batt, D. G., Beaudoin Bertrand, M., Gong, H., Dai, J., Yip, S., Li, P., Sun, D., Wu, D. R., Wang, C., Zhang, Y., Traeger, S. C., Pattoli, M. A., Skala, S., Cheng, L., Obermeier, M. T., Vickery, R., Discenza, L. N., D'Arienzo, C. J., Zhang, Y., Heimrich, E., Gillooly, K. M., Taylor, T. L., Pulicicchio, C., McIntyre, K. W., Galella, M. A., Tebben, A. J., Muckelbauer, J. K., Chang, C., Rampulla, R., Mathur, A., Salter-Cid, L., Barrish, J. C., Carter, P. H., Fura, A., Burke, J. R., and Tino, J. A. (2016) Discovery of 6-Fluoro-5-(*R*)-(3-(*S*)-(8-fluoro-1-methyl-2,4-dioxo-1,2-dihydroquinazolin-3(4*H*)-yl)-2-methylphenyl)-2-(*S*)-(2-hydroxypropan-2-yl)-2,3,4,9-tetrahydro-1*H*-carbazole-8-carboxamide (BMS-986142): A Reversible Inhibitor of Bruton's Tyrosine Kinase (BTK) Conformationally Constrained by Two Locked Atropisomers. *J. Med. Chem. 59*, 9173–9200.

(21) Strödke, B., Gehring, A. P., and Bracher, F. (2015) Synthesis of desaza analogues of annomontine and canthin-4-one alkaloids. *Arch. Pharm. (Weinheim). 348*, 125–131.

(22) Kern, S., Agarwal, S., Huber, K., Gehring, A. P., Strödke, B., Wirth, C. C., Brügl, T., Abodo, L. O., Dandekar, T., Doerig, C., Fischer, R., Tobin, A. B., Alam, M. M., Bracher, F., and Pradel, G. (2014) Inhibition of the SR protein-phosphorylating CLK kinases of Plasmodium falciparum impairs blood stage replication and malaria transmission. *PLoS One 9*, e105732 (1-15).

(23) Nicolae, C. M., Aho, E. R., Choe, K. N., Constantin, D., Hu, H. J., Lee, D., Myung, K., and Moldovan, G. L. (2015) A novel role for the mono-ADP-ribosyltransferase PARP14/ARTD8 in promoting homologous recombination and protecting against replication stress. *Nucleic Acids Res. 43*, 3143–3153.

(24) Iansante, V., Choy, P. M., Fung, S. W., Liu, Y., Chai, J.-G., Dyson, J., Del Rio, A., D'Santos, C., Williams, R., Chokshi, S., Anders, R. A., Bubici, C., and Papa, S. (2015) PARP14 promotes the Warburg effect in hepatocellular carcinoma by inhibiting JNK1-dependent PKM2 phosphorylation and activation. *Nat. Commun. 6*, 7882 (1-15).

(25) Cho, S. H., Ahn, A. K., Bhargava, P., Lee, C.-H., Eischen, C. M., McGuinness, O., and Boothby, M. (2011) Glycolytic rate and lymphomagenesis depend on PARP14, an ADP ribosyltransferase of the B aggressive lymphoma (BAL) family. *PNAS 108*, 15972–7.

(26) Barbarulo, A., Iansante, V., Chaidos, A., Naresh, K., Rahemtulla, A., Franzoso, G., Karadimitris, A., Haskard, D. O., Papa, S., and Bubici, C. (2013) Poly(ADP-ribose) polymerase family member 14 (PARP14) is a novel effector of the JNK2-dependent pro-survival signal in multiple myeloma. *Oncogene 32*, 4231–4242.

(27) Peng, B., Thorsell, A.-G., Karlberg, T., Schüler, H., and Yao, S. Q. (2016) Small Molecule Microarray Based Discovery of PARP14 Inhibitors. *Angew. Chemie Int. Ed. 55*, 1–7.

(28) Yoneyama-Hirozane, M., Matsumoto, S., Toyoda, Y., Saikatendu, K. S., Zama, Y., Yonemori, K., Oonishi, M., Ishii, T., and Kawamoto, T. (2017) Identification of PARP14 inhibitors using novel methods for detecting auto-ribosylation. *Biochem. Biophys. Res. Commun. 486*, 626–631.

(29) Upton, K., Meyers, M., Thorsell, A.-G., Karlberg, T., Holechek, J., Lease, R., Schey, G., Wolf, E., Lucente, A., Schüler, H., and Ferraris, D. (2017) Design and synthesis of potent inhibitors of the mono(ADP-ribosyl)transferase, PARP14. *Bioorg. Med. Chem. Lett. 27*, 2907–2911.

(30) Forst, A. H., Karlberg, T., Herzog, N., Thorsell, A. G., Gross, A., Feijs, K. L. H., Verheugd, P., Kursula, P., Nijmeijer, B., Kremmer, E., Kleine, H., Ladurner, A. G., Schüler, H., and Lüscher, B. (2013) Recognition of mono-ADP-ribosylated ARTD10 substrates by ARTD8 macrodomains. *Structure 21*, 462–475.

(31) Leslie, A. G. W., and Powell, H. R. (2007) Processing Diffraction Data with Mosflm, in *Evolving Methods for Macromolecular Crystallography, 245*, pp 41–51.

(32) Evans, P. R. (2011) An introduction to data reduction: space-group determination, scaling and intensity statistics. *Acta crystallogr. D 67*, 282–292.

(33) McCoy, A. J., Grosse-Kunstleve, R. W., Adams, P. D., Winn, M. D., Storoni, L. C., and Read, R. J. (2007) Phaser crystallographic software. *J. Appl. Cryst. 40*, 658–674.

(34) Emsley, P., Lohkamp, B., Scott, W. G., and Cowtan, K. (2010) Features and development of Coot. *Acta crystallogr. D 66*, 486–501.

(35) Murshudov, G. N., Skubák, P., Lebedev, A. A., Pannu, N. S., Steiner, R. A., Nicholls, R. A., Winn, M. D., Long, F., and Vagin, A. A. (2011) REFMAC5 for the refinement of macromolecular crystal structures. *Acta crystallogr. D 67*, 355–367.

(36) Chen, V. B., Arendall, W. B., Headd, J. J., Keedy, D. A., Immormino, R. M., Kapral, G. J., Murray, L. W., Richardson, J. S., and Richardson, D. C. (2010) MolProbity: all-atom structure validation for macromolecular crystallography. *Acta crystallogr. D 66*, 12–21.

(37) Gehring, A. P., Tremmel, T., and Bracher, F. (2014) One-Pot Conversion of 1-Bromo-β-carboline and 1-Bromocarbazole into Pentacyclic Compounds by Suzuki Cross-Coupling Followed by Spontaneous Cyclization. *Synthesis (Stuttg). 46*, 893–898.

(38) Gibbs-Seymour, I., Fontana, P., Rack, J. G. M., and Ahel, I. (2016) HPF1/C4orf27 Is a PARP-1-Interacting Protein that Regulates PARP-1 ADP-Ribosylation Activity. *Mol. Cell 62*, 432–442.